Supplemental information

Digital twin demonstrates significance of

biomechanical growth control in liver

regeneration after partial hepatectomy

Stefan Hoehme, Seddik Hammad, Jan Boettger, Brigitte Begher-Tibbe, Petru Bucur, Eric Vibert, Rolf Gebhardt, Jan G. Hengstler, and Dirk Drasdo

SUPPLEMENTAL INFORMATION

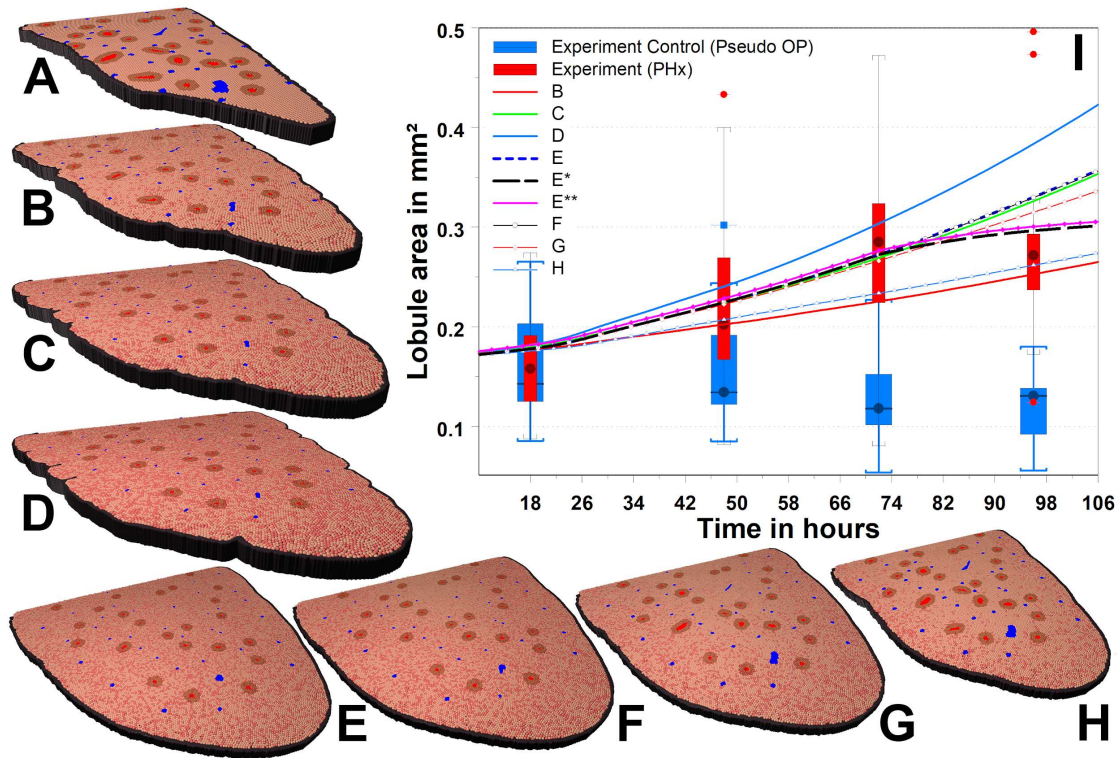## Varying mitotic index and threshold pressure for cell cycle progression.

Figure S1. Parameter sensitivity analysis, related to Figure 4: A) Model of 4 cell layers height constructed from experimental images (see Fig.2) at t=0 days (initial state). B-D) Prediction of liver lobe pattern for different mitotic indices (achieved by varying pressure threshold) at t=3 days. Mitotic index: B) 0.3, C) 0.5 (as found in the experiments) and D) 0.8. Mitotic index = probability of a cell to start proliferating within 24h: Increasing the mitotic index defined as the probability of a cell to start proliferating within 24h (the experimentally found values was 0.5) not only increased the lobe in the simulation (see also (I)), but also led to small undulations at the Glisson capsule (grey color, its Young modulus is 5500Pa) reminiscent of buckling observed in the basal layer of skin or oral mucosa or in irradiated crypts (Drasdo & Loeffler, 2001). Buckling occurs when the stabilizing shear stress (or bending) force is outcompeted by the destabilizing cell proliferation (Drasdo, 2000). The more rigid the Glisson capsule was, the more unlikely was buckling to occur at a certain lobe size. This effect might be tested by increasing the cell cycle progression rate. (E-H) Model predictions for different proliferation inhibition thresholds w after t = 5 days: E) w=300 Pa (leads to a homogeneous distribution of proliferation as found in the experiments, see Fig.3), F) w =200 Pa, G) w = 150 Pa, H) w = 100 Pa. Furthermore, in these simulations the Young-modulus of the capsule was chosen E = 20 kPa. In comparison to A)-D) this led to a smoother Glisson capsule with no undulations. Only one half of the lobe was shown but all simulations were carried out for whole lobes. (E-H) shows that the fraction of cells entering the cell cycle also changed if the pressure threshold, at which a cell would exit the cell cycle, was modified: A lower pressure threshold results in a slower lobule growth speed (see also (I)) but only for w < 200Pa (reference: 300Pa) the deviation was clearly detectable with a half as big lobule increase at day three. The reason is that below w=200Pa the pressure for interior cells is above the proliferation threshold resulting in only growth close to the Glisson capsule (G/H). I) Model kinetics of B)-H) carried out to study the effect of the mitotic index and pressure-based inhibition of proliferation (E*). In the curves E* (black, dashed line) and E** (magenta, solid line) the simulations were carried out with a global inhibition of proliferation once the original liver cell population size has been restored. Therefore, this simulation saturates after 3-4 days while the other simulations do not. In the curve E** (magenta, solid line), the Young's modulus was increased by the factor 30 for small cell-cell distances to study the effect of various cell compressibility. Related to *Results* and *Limitations of the Study*.
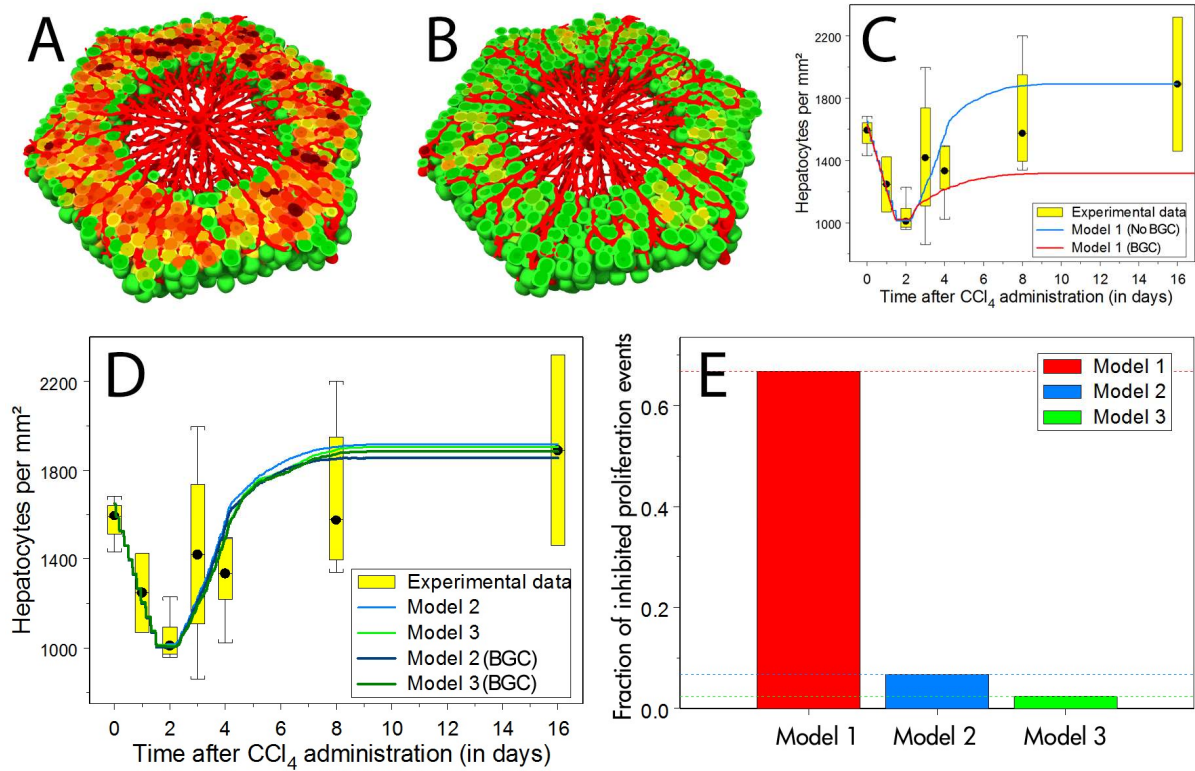
Figure S2. Consistency with liver regeneration after drug-induced liver injury, related to Figure 5: (A) Cell volume during regeneration after CCl$_4$ intoxication if unrealistic compression was not inhibited. (Green = the volume of an isolated sphere, Red = 0.3 times that volume) (B) The same simulation only with the assumption that entrance into the cell cycle is possible only, if the local pressure does not overcome a critical threshold. A Voronoi-based space partitioning analysis has been used to approximate the volume of the hepatocytes in the model. (C) Time course of cell population size per liver lobule in cases (A) and (B). (D): Time course of cell population size per liver lobule in models 2 and 3 with and without pressure inhibition by proliferation (BGC). (E): Fraction of cases in which proliferation impulses do not lead to proliferation due to pressure-controlled growth inhibition for models 1, 2 and 3 showing that the presence of a mechanism that inhibits proliferation by pressure (BGC) does not modify the regeneration dynamics of models 2 and 3 in (Hoehme *et al.*, 2010). Related to *STAR methods*.

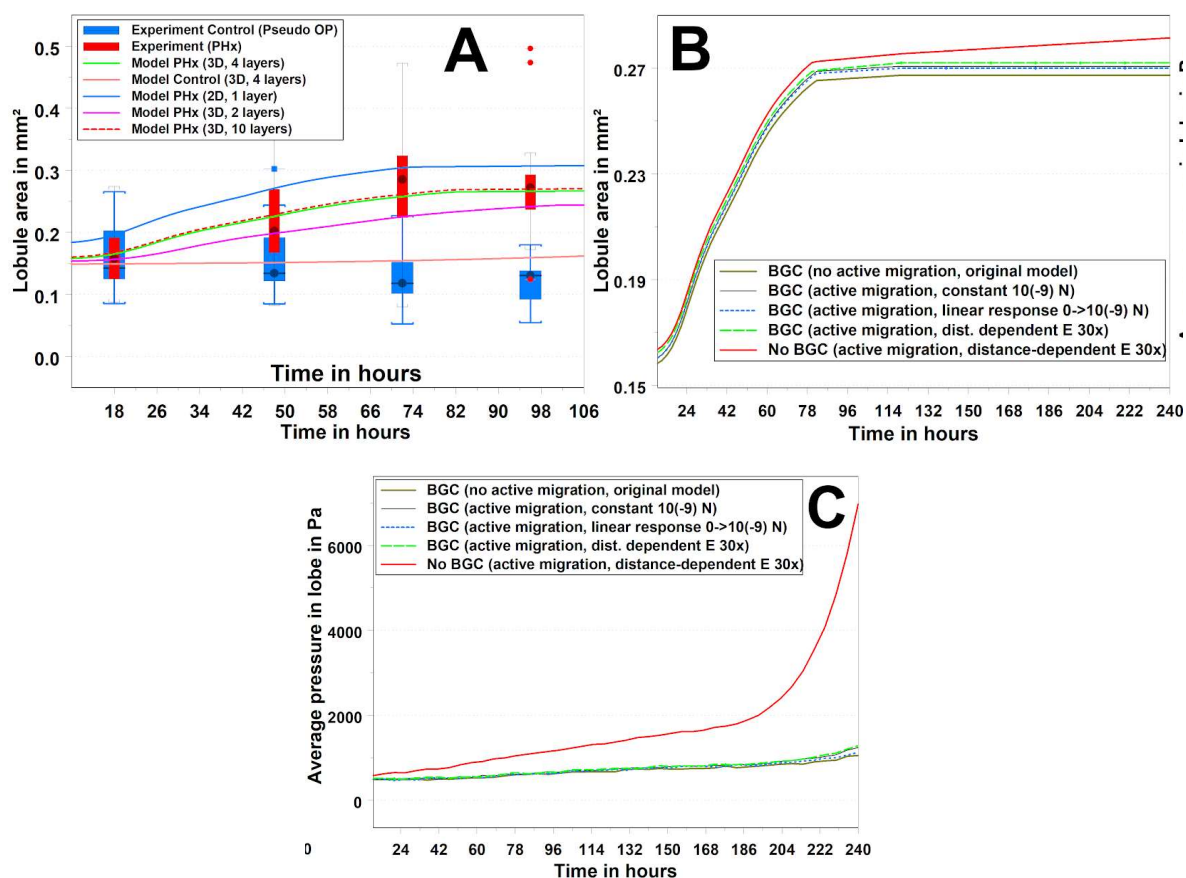# Regeneration simulations varying lobule thickness and other parameters

Figure S3. Effect of lobule thickness on simulation results, related to Figure 2 and STAR Methods: (A) Regeneration vs thickness (z-height) of the simulated lobes (1, 2, 4, 10 cells). (B) Comparison of area increase for different regeneration mechanisms (brown: original model, no active migration towards the Glisson capsule; black, blue, green: active migration towards the Glisson capsule, with constant micromotility force of 10^{-9}N (black), varying migration force (blue), distant-dependent cell Young modulus to mimic the strong repulsive force upon large cell compression (green), absence of BGC but with strong repulsive force upon large cell compression (red). (C) Comparison of average pressure in lobe for the models shown in (B). Related to *STAR methods*.
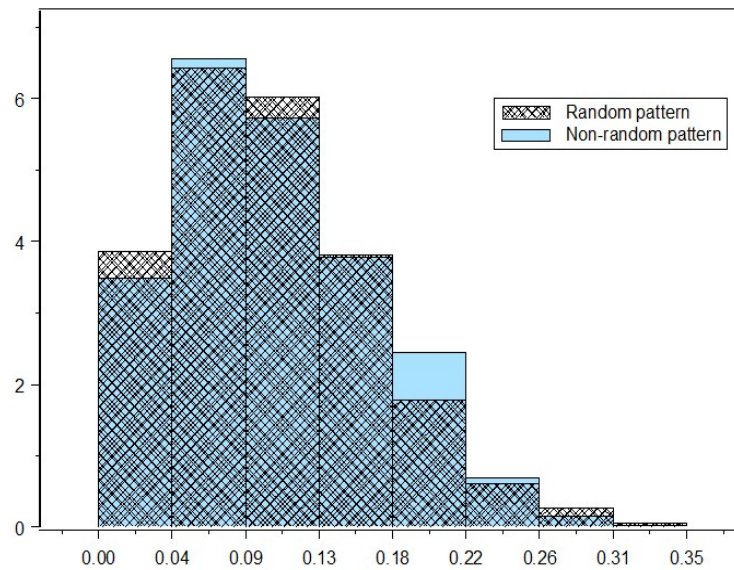
Simulated BrdU proliferating pattern

Figure S4. Number of proliferation neighbors of proliferating cells, related to Figure 5: Frequency histograms for the number of proliferating cells in the vicinity of a proliferating cell predicted by the model for BrdU staining (non-random pattern demarcates the BGC mechanism). BrdU only stains cells in the S-phase, which is about 8h long. Simulated was an experimental standard protocol where mice were sacrificed 2 hours after injection of BrdU. In that case, those cells that were in the S-phase during the injection and those cells that entered the S-phase within the two hours until the mice were sacrificed were BrdU-stained. The simulation results of the histogram equivalent to that in Fig.5C/D for KI-67 staining now shows only minor differences demonstrating that labeling S-phase only is insufficient to detect the BGC-generated specific growth pattern. Related to *STAR methods*.
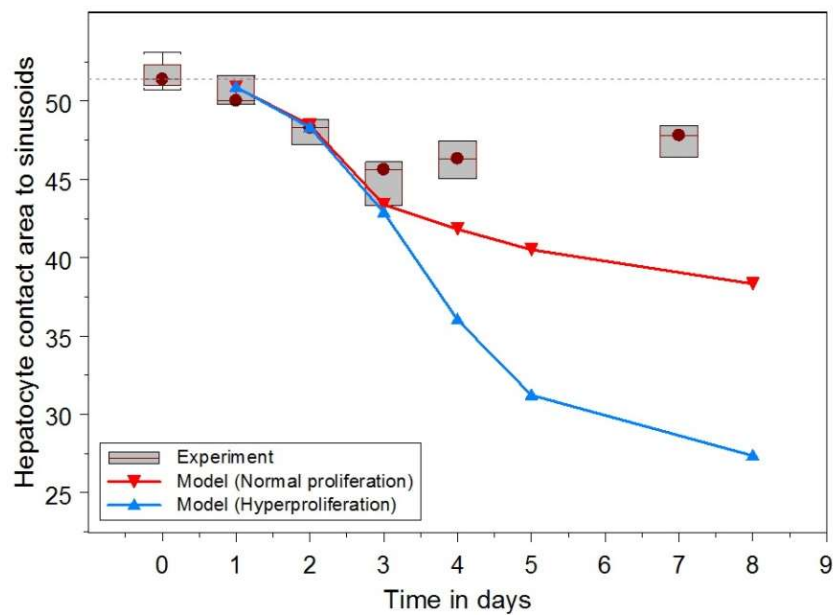
Figure S5. Hepatocyte-sinusoid contact area in regenerating lobe, related to Discussion: Confocal scans of a regenerating liver after PHx indicates a decrease of hepatocyte-sinusoid interface area in the first three days (points) that the model captures quantitatively (red, blue lines). Neo-vascularization results from day 4 in a slow recovery of the hepatocyte-sinusoidal interface area hence the reorganization within the liver lobe is delayed compared to recovery of liver mass, as this was already the case for regeneration after drug-induced liver injury (Hoehme *et al.*, 2010). Our model of the regenerating lobe does not consider neo-vascularization so cannot capture the recovery phase. However, the model predicts that hyperproliferation (blue curve) would not affect the order parameter in the first 3 days after PHx. Related to *Results*.
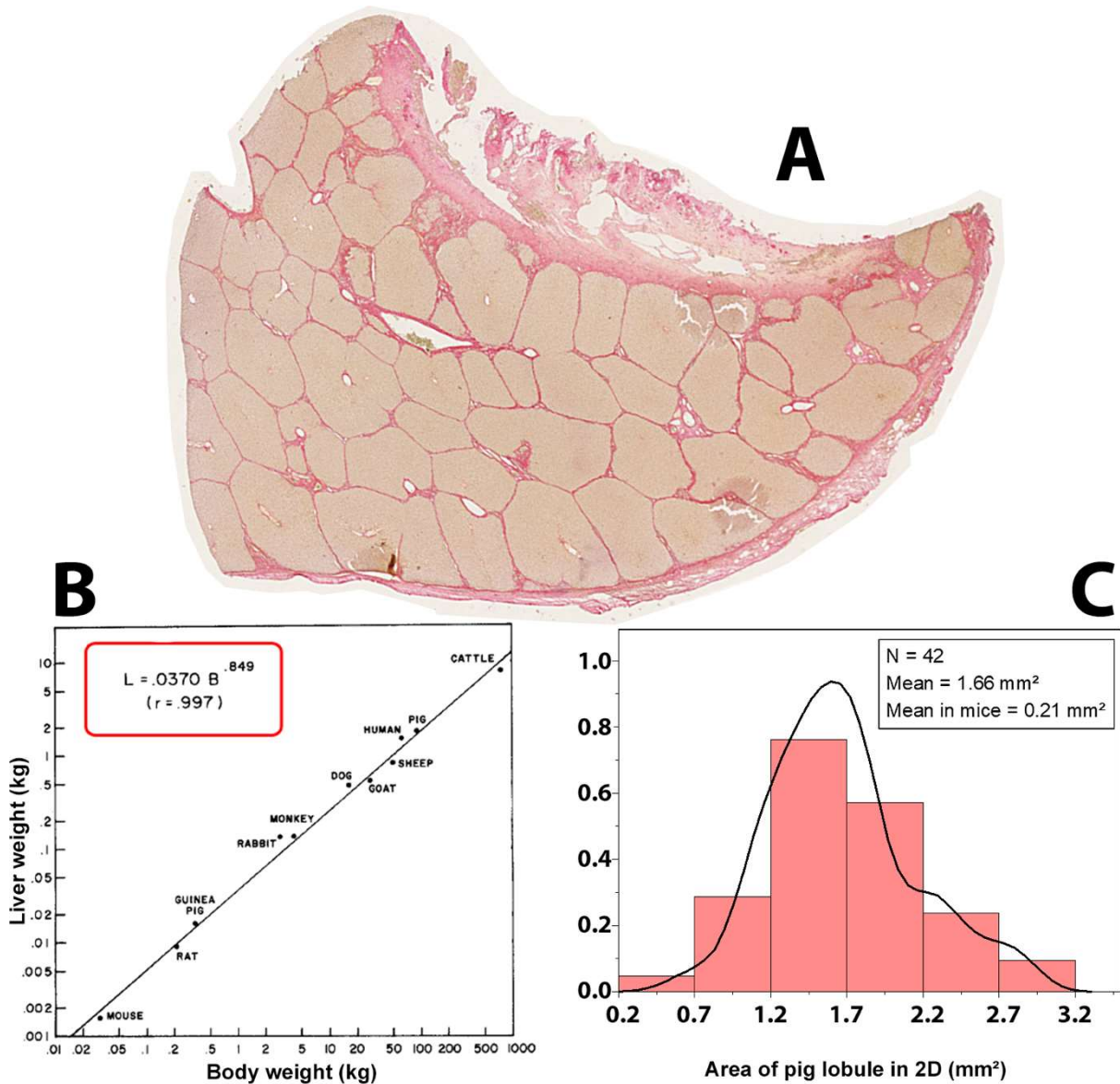
Liver and liver lobule size in pig

Figure S6. Liver architectural parameters in pigs, related to Figure 6: (A) Whole slide scan of a part of a pig liver lobe stained with Sirius Red for collagen in the portal field (B) Liver weight for mice and larger animals, including pig and human. (C) Area of pig liver lobules quantified from images similar to (A). Related to *STAR methods*.

Table S1: Lobule parameters for mouse and pig, related to STAR Methods and all Figures.

Parameter	Mouse		Pig	
	Source	Value ± Standard deviation	Source	Value ± Standard deviation
Number of analyzed datasets	-	26	-	4
Lobule				
Confocal scanning depth	Confocal metadata	95 ± 57 µm	Confocal metadata	60.21 ± 9.11 µm
Lobule height in the model	10 Cell layers	250 ± 0 µm	5 Cell layers	90 ± 0 µm
Lobule area (2D slice)	Bright field microscopy	0.21 ± 0.05 mm²	Bright field whole slides (Sirius Red)	1.66 ± 0.84 mm²
Lobule radius in model (2D slice)	$R = \sqrt{\dfrac{2 \cdot A}{3 \cdot \sqrt{3}}}$ A… lobule area, assuming a regular hexagon	284.3 ± 56.9 µm (12.2 ± 2.4 hepatocytes)	Calculations as in mouse	799.33 ± 260.7 µm (43.0 ± 14.6 hepatocytes)
Area of necrotic lesion before regeneration	Image analysis	0.073 ± 0.011 mm²	-[1]	-
Radius of necrotic lesion before regeneration	$R_{nec} = \sqrt{\dfrac{A_{nec}}{\pi}}$ (assuming a circular necrotic lesion)	149 ± 22 µm (6.4 ± 1.0 hepatocytes)	-[1]	-
Sinusoids				
Radius of sinusoid vessels	Volume analysis	4.75 ± 2.25 µm	Volume analysis	8.85 ± 3.11 µm
Orthogonal minimal vessel distance	Volume analysis	16.45 ± 4.22 µm	Volume analysis	25.7 ± 8.28 µm
Non-branched segment length	Volume analysis	43.1 ± 18.9 µm	-[2]	-
Mean branching angles	Volume analysis	32.5° ± 11.2°	-[2]	-
Vessel volume in lobule	Volume analysis	7.4 ± 1.1%	Volume analysis	11.1 ± 2.6%
Hepatocytes				
Hepatocyte volume	Volume analysis	$1.2653 \cdot 10^{-5} \pm 3.915 \cdot 10^{-6}$ mm³	Volume analysis	$0.6838 \cdot 10^{-5} \pm 8.133 \cdot 10^{-6}$ mm³
Hepatocyte diameter	Volume analysis	23.3 ± 3.1 µm	Volume analysis	18.6 ± 4.7 µm
Hepatocyte density	Image analysis	1889 ± 341 cells/mm²	Volume analysis	2631 ± 397 cells/mm²
Next neighbor distance	Volume analysis	21.6 ± 13.1 µm	Volume analysis	17.4 ± 11.5 µm
Diameter of hepatocyte nucleus	Image analysis	9.3 ± 4.4 µm	-[1]	-
Central vein				
Length in Volume	Volume analysis	107 ± 69 µm	-[1]	-
Radius	Volume analysis	41.2 ± 32.1 µm	Manual analysis	45.3 ± 52.1 µm
Inclination to viewing plane	Volume analysis	6.6° ± 4.1°	-[1]	-
Capsule				
Capsule thickness	Manual analysis (IfaDO, 5 datasets in 2D)	10.75 ± 1.14 µm	Manual analysis (IfaDO, 5 datasets in 2D)	24.96 ± 9.06 µm

[1] Not relevant for current simulations
[2] Not yet possible with current datasets (too limited sinusoid tracking)

Related to *Results*.

Table S2: Simulation parameters, related to STAR Methods and Figures 2, 4, 5, 6 (all simulations).

Parameter / Symbol	Unit	Value (Range in sensitivity analysis)	Source
Cell diameter l_{Cell}	μm	23.3	A
Sinusoid vessel diameter l_{Sinu}	μm	4.75	A
Intrinsic cell cycle time τ	h	24	(Vintermyr & Døskeland, 1987)
Reference energy F_T	J	10^{-16}	(Beysens et al., 2000) (Schienbein et al., 1994)
Hepatocyte Young-Modulus E_{Cell}	Pa	450 (300-1000)	(Davidson et al., 1995) (Lekka et al., 1999)
Sinusoids Young-Modulus E_{Sinu}	Pa	600 (300-1000)	B
Glisson capsule Young-Modulus E_{Gli}	kPa	15 (10-50)	B
Hepatocyte Poisson ratio υ_{Cell}	-	0.4	(Alcaraz et al., 2003) (Mahaffy et al., 2000)
Sinusoids Poisson number υ_{Sinu}	-	0.4	B
Glisson capsule Poisson number υ_{SGli}	-	0.45	B
Hepatocyte diffusion constant D_i^C for all i	cm² s⁻¹	$2 \cdot 10^{-12}$ ($2 \cdot 10^{-13} - 2 \cdot 10^{-11}$)	(Beysens et al., 2000)
Receptor surface density ρ_m For hepatocyte-hepatocyte interaction (Sinusoids are non-adhesive, i.e. $\rho_m = 0$ for interactions involving sinusoids)	m⁻³	$\approx 10^{15}$ ($10^{14} - 10^{16}$)	(Chesla et al., 1998) (Piper et al., 1998)
Binding energy single bond W_s		$\approx 25 k_B T$	(Beysens et al., 2000)
Friction coefficients $\xi_{\parallel}^{CC}$ $\xi_{\perp}^{CC}$ $\xi_{\parallel}^{CS}$ $\xi_{\perp}^{CS}$	Ns / m³	10^7	B
Morphogen diffusion coefficient D_M	cm² / s	10^{-6} (10^{-5}-10^{-7})	(Casciari et al., 1988)
Active migration force F_{AM}	nN	30 (0-100)	B
High compression $\tilde{E}_{ij}(\alpha)$	Pa	450 - 13500 (450-22500)	B
BGC threshold	Pa	675 (475-4500)	B
A … Quantitative analysis of 3D confocal datasets B … Value assumed			
Model parameters. Parameter ranges in parentheses in the last but one column denote the range over which we have varied the respective parameter to test the robustness of our simulation results with regard to the model parameters. Related to STAR methods.			